Chinese Journal of
POLYMER SCIENCE

RESEARCH ARTICLE

https://doi.org/10.1007/s10118-026-3590-0
Chinese J. Polym. Sci.

Spontaneous Gauged O(*N*) Symmetry Breaking in Polymer Crystallization

Mai Zhou, Gui-Qiu Ma, and Zhe Ma*

School of Materials Science and Engineering, Tianjin University, Tianjin 300072, China

Abstract The long-range order and intrinsic entanglement of polymer play a crucial role in crystallization and the corresponding melting relaxation which, however, are rarely treated as a form of symmetry. In this work, a field model is developed based on a self-avoiding random string with open ends, where time dimension for string vibrations is added and the dynamics of chain vibrations is captured by a ϕ^4 theory with O(*N*) symmetry. The long-range order triggered by crystallization is referred to the scalar's breaking in grand canonical ensemble, while entanglement is considered as a geometric dynamic effect in absence of closed loops, rather than chain topology. For the entanglement, there are interactions among the replica scalar's components *via* the gauged O(*N*) symmetry. The infrared stability at $d = 3 + 1$ requires $N = 2$, thus the gauge-scalar theory is reduced to Coleman-Weinberg model in the rest frame. The finite-temperature effect causes the second-order phase transition related to scalar's breaking to become first-order with a metastable region, depending on the gauge coupling g. These modeling results are helpful in understanding the crystallization and melting behavior of polymer, including the difference of the extrapolated temperatures in Gibbs-Thomson equation, and the re-entanglement and the vanishing of long-range order in melt relaxation.

Keywords Crystallization; Spontaneous symmetry breaking; Entanglement; Long-range order

Citation: Zhou, M.; Ma, G. Q.; Ma, Z. Spontaneous gauged O(*N*) symmetry breaking in polymer crystallization. *Chinese J. Polym. Sci.* https://doi.org/10.1007/s10118-026-3590-0

INTRODUCTION

The thermodynamics of semi-crystalline polymer is crucial for disclosing crystallization mechanism and predicting the crystallite structures, which are of great importance to polymer material engineering. However, the microscopic dynamics of polymer has not attracted enough attention yet and the corresponding symmetry-conservation paradigm is not sufficiently explored in polymer crystallization. Meanwhile, the intrinsic entanglement of polymer is rarely addressed from the perspective of conserved dynamics. In addition, the long-range order and entanglement couple to affect the crystallized system *via* the spontaneous symmetry breaking (SSB) in polymer, in which the ground states of the dynamics are not invariant under the global symmetry. Actually, as an important mechanism, the SSB has been shown to interpret many physical behaviors, such as the condensation of the ordered phase in spin system, the formation of superconductor and superfluid, electroweak phase transition and appearance in the Higgs mechanism to give particles their masses.[1,2]

The crystallized polymer's melting behavior could reflect the influence of crystallization on the condensed state of polymer. There are two distinct perspectives that illustrate a long-range order related to the symmetry and the entanglement. One is the Gibbs-Thomson relation from crystallization to final melting and the other is the melt relaxation. However, the entanglement is regarded as the local gauge degree of freedom (d.o.f.) behind the symmetry of the long-range order.

The Gibbs-Thomson equation as a benchmark[3] that describes the relationship between lamellar thickness and undercooling, was proposed based on the classical nucleation kinetics and developed into the second-nucleation kinetics with expanded sample space.[4–7] As described by this equation, the temperature is linearly related to the reciprocal of lamellar thickness. This linear relationship is available for both crystallization and melting processes. However, the corresponding extrapolated temperature T^{∞} for the infinite lamellar thickness are different between crystallization and melting processes, of which the crystallization displays a higher T^{∞} than melting line but is the same with the recrystallization. Extrapolating infinite crystal size leads the two-phase system to reach its thermodynamic limit, where the decreasing of T^{∞} shows the existence of a first-order phase transition explicitly.

What is more peculiar is that this variation of T^{∞} could not be observed in system with α-relaxation,[8] where the segmental transport leads to chain motion to traverse crystals and the supercooled amorphous melt.[9] In this case, the ordering process is either a higher-order phase transition or is completed in crystallization. On the other hand, this ob-

* Corresponding author, E-mail: zhe.ma@tju.edu.cn
Received December 4, 2025; Accepted January 25, 2026; Published online April 16, 2026

served T^{∞} difference attributed to α-relaxation reflects the dynamic property of amorphous phase. It was argued that this T^{∞} difference was associated with the disentanglement by α-relaxation.[10–13] However, it was also found that in poly(propene-*co*-1-octene) copolymers that as 1-octene incorporation increased, the crystallization line remained unchanged while the melting line shifted downwards. It is known that the octene co-units with long pendant groups enhance the entanglement without incorporating into the lattice.[14] This means that the entanglement has a similar influence on both crystallization and melting lines, which is inconsistent with the above case of unchanged crystallization line but decreased melting lines. Thus, entanglement seems not to act as the primary factor responsible for the discrepancy of T^{∞}.

For the Gibbs-Thomson equation, another important factor is the slope, interpreted as the surface energy of chain folding structures between the lamellar and the amorphous region.[3,15] The chain folding and extension at the interface is often regarded as a local order parameter for the segment orientation. The chain extension happens during recrystallization and melting accomplished with crystalline perfection. However, it was reported that in α-relaxation crystals, recrystallization did not happen at sufficiently high crystallization temperatures upon heating,[16] indicating that chain folding at the crystal/amorphase boundary is not a local order but a global orientation in the whole system. This inference is supported by experiments and simulations. The folding structure suddenly arises as soon as the nucleus formation, independent of the degree of polymerization and temperature.[17–21] The chain folding can be also observed prior to the beginning of crystallization.[22] In addition, the long-range order appears in the late period with the continuously increased crystallinity.[23] Actually, this folding behavior at the interface was studied in Gambler's ruin model,[24–26] where the segment configuration at the interface resulted from the chain's random walk. Therefore, the global orientation referred to as long-range order should be responsible for the variation of T^{∞}.

In addition to the Gibbs-Thomson equation, the coupling of entanglement and long-range order could be reflected by the melt relaxation into isotropic and homogeneous state. A two-mode decay process[27,28] and two temperature domains of IIa and IIb divided by self-seeding temperature T_s[29] were observed. The fast relaxation and domain IIb were attributed to re-arrangement of ordered segments[27] and un-melted crystals,[29] while the slow one and domain IIa were attributed to the relaxation of the long-range order.[30] However, the slow relaxation is controlled by the long-chain dynamics through the chain reptation,[30] measured by the longest relaxation time.[31] The longest relaxation time decreases nonlinearly below T_s and exhibits classical diffusion behavior above T_s.[30] According to the Doi-Edwards theory,[32] the entanglement is a geometric constraint that chain's motion is bounded in a tube. The re-entanglement corresponded to tube reformation occurs rapidly below T_s, compared with the slow relaxation of long-range order. Thus, the entanglement is distinct from the long-range order.

So far, there are some investigations performed to model the thermodynamics of crystallized polymer.[33–38] In these models, the free energy was divided into three parts including crystal, melt and interface, which varies in calculating the entropy of entangled supercooled melt and the interface. Not only a comprehensive model of entanglement but also the consideration of long-range order related to the symmetry of polymer were lacking. Ryan and Olmsted[39] considered the long-range order to explain the spinodal decomposition before crystallization. In this work, the Landau free energy also considers crystal and melt, but the chain conformation, where an order parameter η for the chain orientation was introduced. η ranges from 0 to 1 continuously for random coil conformation at zero temperature and helix chain conformation at infinite temperature, and obeys a canonical distribution $\eta = \tanh(\beta E/2)$, where $E = E_0 + \nu\bar{\rho} + \lambda\rho^{\star}$ with $\bar{\rho}$ and $\rho^{\star}$ being the average density and the crystal density, respectively. This η-related term leads to two identical minima of the total free energy[39] at critical temperature for $\nu > 0$, indicating the phase separation of first order, which is typical SSB.

Similarly, Yakunin[40] noticed this broken symmetry in necking process and based on the O(N)-ϕ^4 universal class of the self-avoiding walk (SAW),[41,42] investigated the critical behavior associated with orientation of polymer. In that work, an analogy was made between polymer and spin system, where the self-repulsive interaction corresponds to the coupling between neighboring spins and the external field plays the role of an external magnetic field. The d.o.f. stands for the spin number of closed loops and the dimensionality of the walk is given by the critical exponent. A appearance of magnetization-like order parameter is caused by crystallization in the necking process as external field. This orientation is a second-order phase transition indicated by the divergent effective susceptibility, leading to the argument that the combination of first- and second-order transition observed in the necking process was attributed to spontaneous gauge symmetry breaking or known as the Higgs-Anderson mechanism (*i.e.*, the mass generation of W/Z bosons by a broken scalar doublet in electroweak interaction, where SU(2) × U(1) breaks into $U(1)_s$ and $U(1)_{em}$ breaks into Z_2). He thought that the external field was analogous to the magnetic field, and the electromagnetic field was the U(1) gauge field, thus the external field acting on the ends of polymer was a gauge field. However, it should be noticed that SSB is not spontaneous gauge symmetry breaking. The gauge invariance is not broken and the the external field is even not an intrinsic d.o.f. in his theory, nor in the theory of SAW where no U(1) or SO(N) gauge field was incorporated.

Actually, Yakunin's idea that the external field acting on the ends of polymer is a gauge d.o.f. is consistent with the string theory that the gauge d.o.f. emerges from the boundary conditions of the string.[43] A walk is a random string in Euclidean three-dimension space but without time-like direction. Furthermore, the gauge d.o.f. coincides with the concept of entanglement that the gauge fields can be used to construct non-local observables which are vital in the topological field theory, for the writhe, winding and twine of close loops and links.[44,45] Meanwhile, the mass generation of gauge field in SAW has rich physical meaning. The mass of scalar corresponds to the connectivity of the polymer (m) and it is small

https://doi.org/10.1007/s10118-026-3590-0

due to the polymer's considerable degree of polymerization[46] Therefore, the tree-level mass of gauge field through SSB of scalar is connected to another characteristic length which reflects properties of entanglement. In addition, the topological term at $d=3$ brings the gauge field another mass that does not contradict with the gauge invariance.[44,47] So far, there was one formulation of the SAW theory to incorporate gauge invariance to explain the entanglement for open chains without close loops,[48] where Chern-Simons (CS) terms were introduced for the winding and twine of two chains, and gave a modification of $\lambda^3\phi^6$ term to the effective potential. However, the linking number is not a topological invariant for two intertwined open chains at dimensions $d = 3 + 0$. Then, Ferrari[49] studied links of closed self-avoiding loops to avoid this problem.

In addition, it was disclosed in Ferrari's work[48] that the complex scalar was used for constructing U(1) gauge, which was in contradiction with the O(N) symmetry brought by replica trick.[46] CS terms also can not be kinetic terms of gauge fields,[48] as the theory is formulated in Euclidean space at $d = 3 + 0$ and the CS term is imaginary and appears only as a phase factor. Interestingly, simulation results[28,50] showed that the entanglement density depends on the temperature and the radius of gyration of a single chain increases and the distribution broadens with elevated temperature, following $X^2 \propto T$.[51] Moreover, it is known that in Doi-Edwards' tube model, an important assumption is that the tangent vector along contour coordinate $u = \partial_s X$ satisfies the equivalence between the time and contour coordinates as expressed previously by $u(s + \Delta s, t) = u(s, t + \Delta t)$.[32] It is reasonable to introduce the time dimension into the theory since SAW depends only on s and lacks dynamics. In this case, the periodic boundary condition in time can be induced by finite temperature.[52] The extension is straightforward that in the presence of time, the assumption of random walk along s is still valid due to large degree of polymerization, remaining the linearity of the time-derivative unaffected.

In this work, the gauge d.o.f. is incorporated to dynamic SAW by localizing the global O(N) symmetry. This solves the problem that as a long-range order is necessary for bulk polymers, there is no conserved charge and particle number due to $N \to 0$. Moreover, the renormalization of the induced SO(N) scalar-gauge theory fixes the number the scalar's components by $N=2$ and determines the value of coupling constants, which is crucial to the type of phase transition related to the long-range order. To study this phase transition caused by crystallization at high temperature and in massless limit (infinite-long chain assumption),[2,42] the effective potential at one-loop order is obtained in the grand canonical ensemble, where the chemical potential μ representing the crystallization effect, gives rise to the excited particles and leads to SSB. The Gibbs free energy density can also be successfully derived from the derivative of effective potential with respect to μ.

MODELING AND RESULTS

The Scalar-gauge Theory from SARS

It was proposed by Edwards *et al.*[46] that for the SAW embedded in $\mathbb{R}^3$ at 1 + 0 dimension in vacuum and good solvent, the Hamiltonian (H) is given by

$$\beta H = \lim_{N\to 0}\int \mathrm{d}^3x\left[\frac{1}{2}(\nabla\phi)^2 + \frac{1}{2}m^2\phi^2 + \frac{\lambda}{4!}(\phi^2)^2\right] \tag{1}$$

The mass in quadratic term corresponds to the connectivity by Laplace transformation $\int_0^\infty \mathrm{d}L e^{-m^2L}$, while $\lambda>0$ in the quartic term is the coupling constant for self-repulsion interaction derived from a Dirac δ function-like potential. ϕ is a real N-component scalar with $N \to 0$ brought by replica trick, which leads to a subtle global O(N) symmetry promoted from Z_2. β is the reciprocal temperature ($\beta = 1/T$). In the massless limit, *i.e.*, the infinite long chain approximation, the SSB induced by thermal corrections is known as the Coleman-Weinberg mechanism or dynamic SSB.[1,46,52] This model is invalid for concentrated solution and bulk polymer, where the self-repulsion interaction is screened as $\lambda \to 0$ and the entanglement dominates. However, the effective theory for bulk system is still quartic,[46] implying that the original field theory can be modified for concentrated solution and bulk.

The ϕ^4 theory of SAW was often referred to the Landau-Ginsberg model. However, the ϕ^4 theory has no gauge d.o.f., while the complex scalar is coupled to the U(1) gauge field in the Landau-Ginsberg model. Also, the SAW theory given by Eq. (1) has no explicit time or temperature dependence, while the Landau-Ginsberg model is a statistical field theory ($d=3$). When temperature or time is considered, the later is exactly the Coleman-Weinberg model ($d = 3 + 1$) in Euclidean space.[1] Next, it can be seen that once time dependence is included and the O(N) symmetry is gauged, the renormalization group (RG) drives the SAW ϕ^4 theory precisely to the Coleman-Weinberg model. The action

$$S_0 = \frac{T_s}{2}\int \mathrm{d}t\mathrm{d}s\sqrt{-\det g}\, g^{\alpha\beta}\,\partial_\alpha X^i \partial_\beta X_i \tag{2}$$

with flat metric $g = \mathrm{diag}(-1, 1)$ and finite length $s \in [0, L]$ describes the free string embedded in Euclidean space $X \in \mathbb{R}^d$. The string flexibility is determined by its tension T_s. As expected, the string tension satisfies $T_s = c^{-1} = \left(\frac{\rho}{kb}\right)^{1/2} = \frac{2ad}{b^2}$, where c is the sound velocity of the string, k is the stiffness coefficient, b is a characteristic length, and ρ is the mass density. The bending rigidity a is derived from the free energy composed by quadratic terms of the normal vector $\partial_s^2 X$.[2] Note that b is not the apparent persistence length l_p depending on temperature, and a equals $l_\mathrm{p}T$ by high-temperature in the long-chain approximation.[2] The integration over imaginary time in the action is offset by a, so the end-to-end distance measured in the bulk remains independent on T. This action is continuous version of Rouse dynamics without the random force and periodic boundary condition.[53]

The self-repulsion potential for the interaction is introduced by

$$S_\mathrm{I} = -\frac{u}{2}\int \mathrm{d}t\int \mathrm{d}s\mathrm{d}s'\,\delta^{(d)}(X(s) - X(s')) = -\frac{u}{2}\int \mathrm{d}t\mathrm{d}s\, V[X(s)] \tag{3}$$

where u measuring the excluded volume strength and $[u] = 3 - d$. Thus a simple model is constructed by $S = S_0 + S_\mathrm{I}$ satisfying the random walk along s,

$$-\int \mathrm{d}s\mathrm{d}t\ \frac{d}{2b^2}\left(\partial_s X\right)^2 \Leftrightarrow \left(b^{-1}\partial_s - \frac{1}{2d}\nabla_X^2\right) \tag{4}$$

which is referred to as the action of the self-avoiding random string (SARS). By Wick rotation, $t \to -i\tau$, $S \to S_\mathrm{E}$, the Euclidean action for the bosonic string is

$$S_\mathrm{E} = \frac{a}{2}\int \mathrm{d}\tau\mathrm{d}s\left(\partial_\tau X\right)^2 + \left(\partial_s X\right)^2 + \frac{u}{2}\int \mathrm{d}\tau\mathrm{d}s V\left[X(s)\right] \tag{5}$$

and the partition function is

$$Z = \int_\mathrm{P} DX\, e^{-S_\mathrm{E}} \tag{6}$$

where $\tau \in [0, \beta]$ is the imaginary time and the subscript P denotes the path integral over periodic boundary configurations with $X(s, \beta) = X(s, 0)$.

The two-point Green function $G\left[X(s,\tau),\ X(s',\tau')\right]$ satisfies

$$\begin{aligned}&\left(-2ad\,\partial_\tau^2 + \frac{4a}{b}\,\partial_s - \frac{1}{2d}\nabla_X^2\right)G\left[X(s,\tau),\ X(s',\tau')\right]\\ &= \delta^{(d)}(X - X')\,\delta(s - s')\,\delta(\tau - \tau')\end{aligned} \tag{7}$$

which allows to construct the Hilbert space describing the propagation by S_E between the string' ends, $|X(s,\tau)\rangle \in \mathcal{H}$. Thus, the Green function can be rewritten into the inner product $G\left[X(s,\tau),\ X(s',\tau')\right] = \langle X(s',\tau')|X(s,\tau)\rangle_{S_\mathrm{E}}$ and can be expressed in an alternative representation,

$$\langle X'|\,Z^{-1}e^{-S_\mathrm{E}}|X\rangle = Z^{-1}\int D\phi\, e^{-S[\phi]}\,\phi(X',\tau')\phi(X,\tau) = \langle 0|\,T\phi'\phi|0\rangle \tag{8}$$

where by inserting the unit operator $I = \int \mathcal{D}\phi\,|\phi\rangle\langle\phi|$ and $\langle X|\,|\phi\rangle = \phi(X)$, $\phi^\dagger = \phi$ into the path integral with $\langle 0|$ for the vacuum state generated by $S[\phi]$. The field operator is real and has the dimension $d - 1/2$ and the periodic condition along τ, $\phi(x, 0) = \phi(x, \beta)$, the same with the bosonic string. It is a scalar singlet with Z_2 symmetry.

To convert the self-repulsion interaction into the field theory form, the Hubbard-Stratonovich transformation is introduced to bring the auxiliary field and a related determinant factor appearing in the denominator.[46] Next, the derivative respect to s is replaced by m^2 by the Laplace transformation. Applying replica trick to the denominator and integrating out the auxiliary field, the Lagrangian can be obtained as follows

$$\mathcal{L}_\mathrm{E} = \lim_{N\to 0} ad\left(\partial_\tau\phi\right)^2 + \frac{a}{d}\left(\partial_s\phi\right)^2 + 2am^2\phi^2 + \frac{u}{8}\left(\phi^2\right)^2 \tag{9}$$

where the replica scalar field $\phi = \left(\phi_1, \phi_2, \ldots, \phi_N\right)$, $\phi^2 = \sum_{i=1}^N \phi_i^2$ with $[\phi] = 1$, $[u] = 0$ at $d = 3$. Then assigning

$$\begin{aligned} x &\to d^{-1}x\\ m^2/d &\to m^2\\ u/16ad &\to \lambda/4!\\ 2a/d^{d-1} &= \bar{h}^{-1}\end{aligned} \tag{10}$$

the Lagrangian becomes

$$\mathcal{L}_\mathrm{E} = \frac{1}{2}\left(\partial_\mathrm{E}\phi\right)^2 + \frac{1}{2}m^2\phi^2 + \frac{\lambda}{4!}\left(\phi^2\right)^2 \tag{11}$$

and the partition function is

$$Z = \lim_{N\to 0}\int_\mathrm{P} D\phi\, e^{-\frac{1}{\bar{h}}\int_{X,\tau}\mathcal{L}_\mathrm{E}} \tag{12}$$

The original Z_2 symmetry is promoted to O(N) symmetry. Now Eq. (11) is the field theory of the oscillating self-avoiding random string.

Because of the appearance of the long range order, a substantive conserved charge in the bulk is required. This means that the limit $N \to 0$ is no longer valid; instead, the theory requires $N \geq 2$. Furthermore, extending the global O(N) symmetry into a local gauge one gives rise to additional coupling among replica components. After a Wick rotation backward to the dynamics, the Lagrangian is

$$\mathcal{L} = -\frac{1}{2}\mathrm{tr}\left(F^{\mu\nu}F_{\mu\nu}\right) - \frac{1}{2}\left(D_\mu\phi\right)^2 - \frac{1}{2}m^2\phi - \frac{\lambda}{4!}\left(\phi^2\right)^2 \tag{13}$$

where $D_\mu = \partial_\mu - igA_\mu^a t^a$ is covariant derivative and $t^a = iT^a$ is the pure imaginary generator of the fundamental representation of SO(N) group. The coupling constant g represents the strength of gauge interaction. As for $\mathrm{tr}\left(F^{\mu\nu}F_{\mu\nu}\right) = F_{\mu\nu}^a F^{a,\mu\nu}\mathrm{tr}\left(t^a t^b\right)$, the field strength tensor is $F_{\mu\nu}^a = \partial_\mu A_\nu^a - \partial_\nu A_\mu^a + gf^{abc}A_\mu^b A_\nu^c$. Here $f^{abc} \in \mathbb{R}$ is the group structure constant. The partition function becomes

$$Z = \int DA\, D\phi\, e^{iS} \tag{14}$$

in natural units ($\bar{h} = c = k = 1$). Let $g \to \sqrt{2}g$, $A \to A/\sqrt{2}$, and choose $C(N) = 1$ for the trace normalization of $SO(N)$, the Lagrangian becomes

$$\mathcal{L} = -\frac{1}{4}\mathrm{tr}\left(F^{\mu\nu}F_{\mu\nu}\right) - \frac{1}{2}\left(D_\mu\phi\right)^2 - \frac{1}{2}m^2\phi - \frac{\lambda}{4!}\left(\phi^2\right)^2 \tag{15}$$

The standard formation of SO(N) scalar-gauge theory is now obtained with g and λ both dimensionless at $d = 3 + 1$. This theory is nonrelativistic for bulk polymers in the rest frame, where $c = 1$ stands for the sound velocity and ϕ only has translation invariance and spatial rotation invariance besides the O(N) symmetry. Therefore, the conservation of energy, momentum, and particle number ensures the validity of using the grand canonical ensemble in the next sections.

Renormalization Group

Both coupling constants g and λ should not be extremely large in the bulk, then the perturbative method of renormalization is applicable. The renormalization is performed at zero temperature, since the possible topological term does not influence the dynamics in the bulk at $d = 4$.[44] Faddeev-Popov procedure is used for gauge fixing in the Feynman gauge, and one-loop diagrams are calculated with counterterms. Then, the β-function is obtained[1] by using the identities among these one-loop counterterms and the property of lie algebra $SO(N)$. The β-functions are

$$\beta(\lambda) = \frac{\lambda^2(N+8)}{9(4\pi)^2} + \frac{4g^2(N-1)(3g^2-\lambda)}{(4\pi)^2} \tag{16}$$

$$\beta(g) = -\frac{g^3}{(4\pi)^2}\left[\frac{11}{3}(N-2) - \frac{1}{3}\right] \tag{17}$$

Comparing with the ungauged theory, an additional term $\frac{4g^2(N-1)(3g^2-\lambda)}{(4\pi)^2}$ appears in $\beta(\lambda)$. It is known that the 1/2 scaling law of the random walk indicates an almost free behavior widely observed within the bulk polymer system, where the repulsive interaction along the contour is screened by adjacent monomers, *i.e.*, $\lambda \ll 1$, and the repulsion length scale is of order $\lesssim b$. This additional term accounts for the strengthened screening of λ with $3g^2 > \lambda$ for $N \geq 2$, implying

that g should be larger than λ, that is to say, the entanglement becomes much stronger than the repulsion.

For $N > 2$ and $\beta(g) < 0$, only one scalar species contributes $1/3$, implying asymptotic freedom in the U.V. regime, and large N reinforce the ultraviolet freedom of the theory. The asymptotic freedom seems satisfactory, which leads to free behavior with interaction in short distance, while chains are disentangled in short distance and the entanglement becomes stronger in large distance. However, the asymptotic freedom will also lead to the unexpected problem of charge confinement and charged bosons.

On the other hand, it can be indicated from the β functions that coupling constants do not flow to any nontrivial fixed point at $d = 4$. However, with small ε-expansion, *i.e.*, the spacetime dimension d shifting to $\varepsilon = 4 - d \ll 1$,[1] the β-functions are also shifted by $-\varepsilon\frac{\lambda}{3}$ and $-\frac{\varepsilon}{2}g$, which yields renormalization group (RG) flows in the (λ, g^2) plane.

For $N > 2$, $\beta(g) < 0$ causes the Gaussian fixed point $g = 0$ toward U.V., while λ admits the usual Wilson-Fisher fixed point in I.R. However, g grows toward I.R. and affects λ significantly. For the weak coupling, only the linear terms are dominant, so $\beta(g) \approx -\frac{\varepsilon}{2}g$ and $\beta(\lambda) \approx -\varepsilon\lambda$, and the flow of (λ, g^2) approaches $(0, 0)$, the Gaussian fixed point in the U.V. For $g \equiv 0$, gauge interactions are not even included, regardless of whether in the U.V. or I.R. regime, thus it should be abandoned. When g becomes non-negligible in the I.R. regime, the g-dependent contribution to $\beta(\lambda)$ is approximately proportional to $g^2(3g^2 - \lambda)$. This alters the λ-flow and its fixed-point structure obviously, driving the system into the strong-coupling regime beyond one-loop order, which exceeds the validity of perturbation method.

Therefore, $N = 2$ is required to maintain the I.R. stability of the theory at one-loop order. In this case, the scalar-gauge theory reduces to the Coleman-Weinberg model, *i.e.*, scalar QED[1] without the Lorentz symmetry. The RG flow for $N = 2$ is shown in Fig. 1. The RG flows toward two distinct I.R. stable regimes and the area of $g^2 \gg \lambda$ enlarges with increasing ε, reflecting the much stronger gauge interaction for the entanglement compared with the repulsion among monomers. This explains the almost free behavior with small λ and the entanglement-dominant interaction in bulk polymer.

In addition to infrared stability, the assignment of $N=2$ is also based on the physical interpretation of the conserved SO(N) charge with charge confinement for $N>2$. According to Eq. (8), the physical states correspond to the ends of the string, thus the associated conserved charge represents the ends' number. Within a finite volume, this charge equals to the net flux across the boundary, accounting for chains exiting through extension at the interface. As a result, the boundary configurations of chain folding/extension emerge to man-

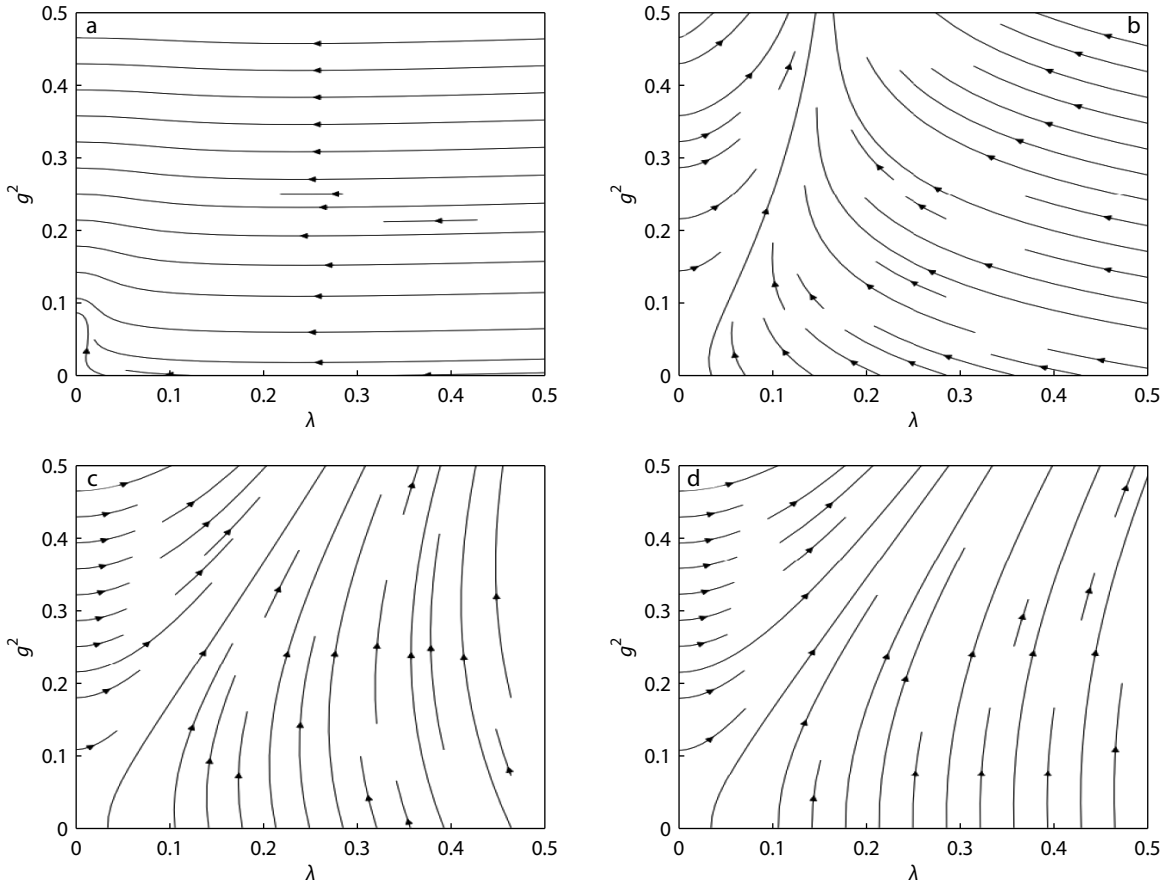

Fig. 1 The renormalization group flow of the Coleman-Weinberg model at $d = 4 - \varepsilon$, shown in subplots for ε being (a) 0.001, (b) 0.01, (c) 0.1, and (d) 1.

https://doi.org/10.1007/s10118-026-3590-0

ifest charge conservation.

Since local folding/extension are also observed, especially in the samples exhibiting α-relaxation,[10–12,54–60] the corresponding charge cannot be confined. Otherwise, only charge singlets are physically accessible[1,61] and the local folding/extension events can not be observed. Moreover, for $N > 2$, the gauge bosons carry the same charge as the scalar due to $f^{abc} \neq 0$, while the experimental results showed that the entanglement is dynamical and not conserved. It is indicated that the gauge field should not contribute to the conservation of the particle number of the scalar.

The Effective Potential at Finite Temperature

The infinite-long chain and high-temperature approximation,[2] *i.e.*, $\beta m \ll 1$, is employed to calculate the effective potential with the background method.[1,52] The temperature range of interest is approximately $T = 200-500$ K. For polymer, the monomer size of order 10^{-10} m, corresponds to the length scale $l = 10^{-6}-10^{-4}$ m for the whole chain with the approximate sound velocity $v = 3\times10^{3}$ m·s^{-1}. To estimate the magnitude, it is reasonable to take

$$\begin{gathered} v = 3\times10^{3}\ \mathrm{m\cdot s^{-1}}, \quad \hbar v = 1.97\times10^{-9}\ \mathrm{meV\cdot m} \\ T = 200\ \mathrm{K}, \quad kT = 17.2\ \mathrm{meV} \\ l = 1\times10^{-6}\ \mathrm{m} \end{gathered} \tag{18}$$

Then, the maximum of βm is estimated by

$$\beta m = \frac{1.97\times10^{-9}}{17.2\times1\times10^{-6}} = 1.15\times10^{-4} \tag{19}$$

which is negligibly small, much less the normal βm range $10^{-7}-10^{-5}$.

Notably, this approximation also holds for the chemical potential μ, where corrections are dominated by thermal fluctuations. The chemical potential corresponds to the lamellar thickness determined by the Gibbs-Thomson relation. The correlation length satisfies $\xi \geq 5\times10^{-9}$ m and the Gibbs-Thomson relation remains valid even under a supercooling of 100 K. For a typical critical crystallization temperature $T = 400$ K, a supercooling 100 K, and a correlation length $\xi = 1\times10^{-8}$ m, the estimated $\beta\mu$ value in the critical region is

$$\beta\mu = \frac{1.475\times10^{-1}}{25.85} \simeq 10^{-3}-10^{-2} \tag{20}$$

Thus, the typical range is $\beta\mu = 10^{-4}-10^{-3}$. Although μ is relatively large compared with m, $\beta\mu$ remains small, ensuring the validity of the infinite-long chain approximation and the high-temperature expansion in loop calculations.

Different from the zero-temperature case,[1] the Matsubara summation[52] at finite temperature not only introduces temperature dependence but also yields contributions of order $O\left(m^4\left(C_1\ln(m^2/T^2)+C_2\right)\right)$ which modify the vacuum energy. C_1, C_2 are constants determined by the vacuum energy renormalization conditions.

For $N = 2$, let $\phi = \frac{1}{\sqrt{2}}(\phi_1 + i\phi_2)$. The Lagrangian is then given by standard form of Coleman-Weinberg model,

$$\mathcal{L} = -\frac{1}{4}F^{\mu\nu}F_{\mu\nu} + \frac{1}{2}(D\phi)^{\dagger}(D\phi) - m^2\phi^{\dagger}\phi - \frac{\lambda}{6}(\phi^{\dagger}\phi)^2 \tag{21}$$

With the introduced chemical potential for $D_0 \to D_0 - i\mu$, the Lagrangian becomes

$$\mathcal{L} \to \mathcal{L}\left[m^2 \to m^2 - \mu^2\right] + \mu\mathcal{N} \tag{22}$$

where $\mathcal{N}$ is the particle number density given by conserved current $J^{a\mu} = -\frac{i}{2}g\left[(\partial^{\mu}\phi)^T t^a\phi - (t^a\phi)^T\partial^{\mu}\phi\right]$ for $\mu = 0$. Assuming $m^2 = 0$, applying the background field method to the complex scalar field, $\phi = \varphi_{\mathrm{cl}} + \varphi_1 + i\varphi_2$, leads to the expansion in the Landau gauge $\xi = 0$,

$$\begin{aligned} \mathcal{L} = & -\left(-\mu^2\right)\varphi_{\mathrm{cl}}^2 - \frac{\lambda}{6}\varphi_{\mathrm{cl}}^4 \\ & + \frac{1}{2}A^{\mu}\left[(\partial^2 + 2g^2\varphi_{\mathrm{cl}}^2)g_{\mu\nu} - \partial_{\mu}\partial_{\nu}\right]A^{\nu} \\ & + \varphi_1\left[-\partial^2 - (-\mu^2) - \lambda\varphi_{\mathrm{cl}}^2\right]\varphi_1 \\ & + \varphi_2\left[-\partial^2 - (-\mu^2) - \frac{\lambda}{3}\varphi_{\mathrm{cl}}^2\right]\varphi_2 \\ & - \frac{\lambda}{6}\varphi_1^4 - \frac{2\lambda}{3}\varphi_{\mathrm{cl}}\varphi_1^3 - \frac{\lambda}{3}\varphi_1^2\varphi_2^2 - \frac{2\lambda}{3}\varphi_{\mathrm{cl}}\varphi_1\varphi_2^2 - \frac{\lambda}{6}\varphi_2^4 \\ & + g^2A_{\mu}^2\varphi_1^2 + g^2A_{\mu}^2\varphi_2^2 + 2g^2A_{\mu}^2\varphi_1\varphi_2 \\ & + 4\mu\phi_2\partial^0\phi_1 \end{aligned} \tag{23}$$

where φ_{cl} is the classical field and φ_1, φ_2 are fluctuations integrated out. The gauge fixing $\xi = 0$ also implies $\partial_{\mu}A^{\mu} = 0$, so all cross terms involving derivatives of A and ϕ vanish. The last term $4\mu\phi_2\partial^0\phi_1$ originates from the particle number density and contributes the vacuum correlation. The mass parameters in the above expression are

$$m_1^2 = -\mu^2 + \lambda\varphi_{\mathrm{cl}}^2 \tag{24}$$

$$m_2^2 = -\mu^2 + \frac{\lambda}{3}\varphi_{\mathrm{cl}}^2 \tag{25}$$

$$m_a^2 = 2g^2\varphi_{\mathrm{cl}}^2 \tag{26}$$

The perturbative effective potential at one-loop order is given by

$$\begin{aligned} \mathcal{V}_{\mathrm{eff}} = & -\mu^2\varphi_{\mathrm{cl}}^2 + \frac{\lambda}{6}\varphi_{\mathrm{cl}}^4 \\ & + \frac{m_1^4}{64\pi^2}\left[\ln\frac{m_1^2}{M_1^2} + C_1 + 2\ln4\pi - 2\gamma\right] + \frac{m_1^2T^2}{24} \\ & + \frac{m_2^4}{64\pi^2}\left[\ln\frac{m_2^2}{M_2^2} + C_2 + 2\ln4\pi - 2\gamma\right] + \frac{m_2^2T^2}{24} \\ & + \frac{3m_a^4}{64\pi^2}\left[\ln\frac{m^2}{M_a^2} + C_a + 2\ln4\pi - 2\gamma\right] + \frac{m_a^2T^2}{8} \\ & + \frac{2\mu^2}{m_1^2 - m_2^2}\left\{\frac{m_1^4}{64\pi^2}\left[\ln\frac{m_1^2}{M_1^2} + C_1 - 2 + 2\ln4\pi - 2\gamma\right] - \frac{m_1^2T^2}{24}\right. \\ & \left. - \frac{m_2^4}{64\pi^2}\left[\ln\frac{m_2^2}{M_2^2} + C_2 - 2 + 2\ln4\pi - 2\gamma\right] + \frac{m_2^2T^2}{24}\right\} \end{aligned} \tag{27}$$

which only retains those terms relying on μ and φ_{cl}. The coefficients C and M^2 are determined by the tree-level minimum $\varphi^{\star}$ at $T = 0$ with $\varphi^{\star 2} = 3\frac{\mu^2}{\lambda}$, using the vacuum energy renormalization conditions. Let

$$C_1 = C_2 = C_{\mathrm{s}} \tag{28}$$

$$M_1^2 = m_1^2\left(\varphi_{\mathrm{cl}} = \varphi^{\star}\right) = 2\mu^2 \tag{29}$$

$$M_a^2 = m_2^2\left(\varphi_{\mathrm{cl}} = \varphi^{\star}\right) = \frac{6g^2\mu^2}{\lambda} \tag{30}$$

while M_2^2 remains undetermined. The extremum condition yields

$$C_s = -2\ln 4\pi + 2\gamma + \frac{1}{5}, \quad C_s = -2\ln 4\pi + 2\gamma - \frac{1}{2} \tag{31}$$

Since $\lambda\varphi_{cl}^2 \sim O(\mu^2)$, the last term in Eq. (27) can be replaced by the derivative with respected to $\lambda\varphi_{cl}^2$:

$$\frac{\mu^2\left(-\mu^2+\frac{2\lambda}{3}\varphi_{cl}^2\right)}{32\pi^2}\left[2\ln\frac{-\mu^2+\frac{2\lambda}{3}\varphi_{cl}^2}{2\mu^2}-\frac{13}{5}\right]-\frac{\mu^2T^2}{6} \tag{32}$$

The effective potential now becomes

$$\begin{aligned}\mathcal{V}_{\text{eff}}\left(\varphi_{cl},\mu,T\right) = &-\mu^2\varphi_{cl}^2+\frac{\lambda}{6}\varphi_{cl}^4\\ &+\frac{\left(-\mu^2+\lambda\varphi_{cl}^2\right)^2}{64\pi^2}\left(\ln\frac{-\mu^2+\lambda\varphi_{cl}^2}{2\mu^2}+\frac{1}{5}\right)\\ &+\frac{\left(-\mu^2+\frac{\lambda}{3}\varphi_{cl}^2\right)^2}{64\pi^2}\left(\ln\frac{-\mu^2+\frac{\lambda}{3}\varphi_{cl}^2}{2\mu^2}+\frac{1}{5}\right)\\ &+\frac{3g^4\varphi_{cl}^4}{16\pi^2}\left(\ln\frac{\lambda\varphi_{cl}^2}{3\mu^2}-\frac{1}{2}\right)\\ &+\frac{\mu^2\left(-\mu^2+\frac{2\lambda}{3}\varphi_{cl}^2\right)}{32\pi^2}\left(2\ln\frac{-\mu^2+\frac{2\lambda}{3}\varphi_{cl}^2}{2\mu^2}-\frac{13}{5}\right)\\ &+\left(\frac{g^2T^2}{4}+\frac{\lambda T^2}{18}\right)\varphi_{cl}^2-\frac{\mu^2T^2}{6}\end{aligned} \tag{33}$$

Here, the thermal mass arising from the scalar field is $m_T^2 = \frac{g^2T^2}{4}+\frac{\lambda T^2}{18}$, which can be verified by calculating the scalar field thermal self-energy *via* the four-point vertexes. Similar with the zero-temperature case, only the four-point vertex contributes to the gauge field thermal self-energy in the Landau gauge. The self-energy of the gauge field is given by

$$\Pi^{\mu\nu} = -g^2\frac{T}{V}\sum\nolimits_K\left[D_1(K)+D_2(K)\right]2g^{\mu\nu} \tag{34}$$

Due to the only O(3) symmetry of the spatial rotation, the determination of the thermal mass requires constructing the four-dimensional tensor basis for the thermal self-energy using three-dimensional projection operators.[52] It is worth noting that a static condition to the self-energy is also added to obtain equations for four unknown components, *i.e.*, the following equation set,

$$\begin{cases} N_\mu N_\nu \Pi^{\mu\nu} = \Pi_L N^2 \\ Q_\mu Q_\nu \Pi^{\mu\nu} = \Pi^L Q^2 \\ g_{\mu\nu}\Pi^{\mu\nu} = 2\Pi_T + \Pi_L + \Pi^L \\ \Pi_L + \Pi^L = 2\Pi_T + \Pi_C \end{cases} \tag{35}$$

where N and Q denote the three- and four-dimensional momenta, respectively. The subscripts L and T represent the three-dimensional longitudinal and transverse polarizations, respectively, while the superscript L corresponds to the four-dimensional longitudinal component. The symbol C denotes the mixed mode composed of both the three-dimensional and four-dimensional longitudinal degrees of freedom. Thus, the resulting thermal self-energy of the gauge field is $\frac{g^2T^2}{6}$ rather than $\frac{g^2T^2}{3}$, since it is evenly distributed between the three-dimensional longitudinal and the four-dimensional longitudinal components. This ensures the three-dimensional transverse modes to acquire the same thermal self-energy once the two longitudinal d.o.f. are removed. As a result, all three polarization directions of the vector field acquire the same thermal mass $m_D^2 = \frac{g^2T^2}{6}$.[52]

In the infrared-stable regime of the *RG* flow with $\lambda < g^2$, there are two relevant limits for coupling constants. For $\lambda < 3g^2 \ll 1$ and $\lambda \ll g^2 \ll 1$, the $O(\mu^3 T)$ terms are negligible and consequently all logarithmic terms are negligible. For $\lambda \ll g^2 < 1$, the logarithmic term of gauge-field vacuum modification remains and affects the critical behavior. However, for $\lambda \ll g^2 \ll 1$, the critical behavior is changed by considering the next-leading-order corrections from ring resummation.[52] The successive loops are involved in ring resummation, giving rise to nonperturbative effects in shaping the effective potential especially at high temperature.[52] The correction from ring resummation is given by

$$\mathcal{V}_{\text{ring}} = d_i\frac{T}{8\pi}m_i m_{i,T}^2 - \frac{T}{12\pi}\left[\left(m_i^2+m_{i,T}^2\right)^{\frac{3}{2}}-m_i^3\right] \tag{36}$$

where m_i and $m_{i,T}$ denotes the mass and thermal mass of arbitrary species i in the system; d_i is the d.o.f. of species i. Substituting Eq. (36) yields the effective potential with subleading corrections.

$$\begin{aligned}\mathcal{V}_{\text{eff}}\left(\varphi_{cl},\mu,T\right) = &-\mu^2\varphi_{cl}^2+\frac{\lambda}{6}\varphi_{cl}^4\\ &+\frac{\left(-\mu^2+\lambda\varphi_{cl}^2\right)^2}{64\pi^2}\left(\ln\frac{-\mu^2+\lambda\varphi_{cl}^2}{2\mu^2}+\frac{1}{5}\right)\\ &+\frac{\left(-\mu^2+\frac{\lambda}{3}\varphi_{cl}^2\right)^2}{64\pi^2}\left(\ln\frac{-\mu^2+\frac{\lambda}{3}\varphi_{cl}^2}{2\mu^2}+\frac{1}{5}\right)\\ &+\frac{3g^4\varphi_{cl}^4}{16\pi^2}\left(\ln\frac{\lambda\varphi_{cl}^2}{3\mu^2}-\frac{1}{2}\right)\\ &+\frac{\mu^2\left(-\mu^2+\frac{2\lambda}{3}\varphi_{cl}^2\right)}{32\pi^2}\left(2\ln\frac{-\mu^2+\frac{2\lambda}{3}\varphi_{cl}^2}{2\mu^2}-\frac{13}{5}\right)\\ &+\left(\frac{g^2T^2}{4}+\frac{\lambda T^2}{18}\right)\varphi_{cl}^2-\frac{\mu^2T^2}{6}\\ &+\frac{T}{8\pi}\left(-\mu^2+\lambda\varphi_{cl}^2\right)^{\frac{1}{2}}\left(\frac{g^2T^2}{4}+\frac{\lambda T^2}{18}\right)\\ &-\frac{T}{12\pi}\left(-\mu^2+\lambda\varphi_{cl}^2+\frac{g^2T^2}{4}+\frac{\lambda T^2}{18}\right)^{\frac{3}{2}}\\ &+\frac{T}{8\pi}\left(-\mu^2+\frac{\lambda}{3}\varphi_{cl}^2\right)^{\frac{1}{2}}\left(\frac{g^2T^2}{4}+\frac{\lambda T^2}{18}\right)\\ &-\frac{T}{12\pi}\left(-\mu^2+\frac{\lambda}{3}\varphi_{cl}^2+\frac{g^2T^2}{4}+\frac{\lambda T^2}{18}\right)^{\frac{3}{2}}\\ &+\frac{3T}{8\pi}\left(2g^2\varphi_{cl}^2\right)^{\frac{1}{2}}\left(\frac{g^2T^2}{6}\right)-\frac{T}{4\pi}\left(2g^2\varphi_{cl}^2+\frac{g^2T^2}{6}\right)\end{aligned} \tag{37}$$

For $\lambda < 3g^2 \ll 1$, all logarithmic and secondary corrections can be neglected as mentioned before. However, for $\lambda \ll g^2$, the situation changes even with small coupling constants. In this case, both the ring resummation and logarithmic terms must be retained in the quartic term, since $\frac{9g^4}{8\pi^2\lambda}$ is not negligible. As the quartic term becomes comparable to the quadratic term and the non-perturbative ring corrections

near small field values, their interplay can largely modify the effective potential.

Nevertheless, it is difficult to tune these parameters to make all these terms the same order of magnitude within the classical field values. Even though the logarithmic term is important in the low-field regime, its contribution is suppressed by the quartic mass prefactor. This implies that only two separate cases need to be analyzed, which include only the logarithmic and the ring resummation contribution separately. It might be possible that these two contributions become comparable for $g \le 10^{-3}$, $\lambda^2 \ll g^2$ and $\frac{9g^4}{8\pi^2\lambda} = O(0.1) - O(10)$ or even larger. These parameters are excessively restrictive and even physically unrealistic, considering that g^2/λ approaches the infrared stable regime.

The Critical Behavior for Different Coupling Constants

Considering thermal masses only, the effective potential is given by

$$\mathcal{V}_{\text{eff}} = (m_T^2 - \mu^2)\varphi_{\text{cl}}^2 + \frac{\lambda}{6}\varphi_{\text{cl}}^4 - \frac{\mu^2 T^2}{6} \tag{38}$$

where $m_T^2 = \frac{1}{4}g^2T^2 + \frac{1}{18}\lambda T^2$. Assigning $x^2 = \frac{\lambda\varphi_{\text{cl}}^2}{3\mu^2}$, the effective potential is rewritten into $\mathcal{V}_{\text{eff}} = \frac{3\mu^4}{2\lambda}x^2\left[2\left(\frac{m_T^2}{\mu^2} - 1\right) + x^2\right]$. The potential is plotted as a function of T in Fig. 2.

Now the critical point is given by $T_c = \frac{\mu}{\sqrt{\frac{g^2}{4} + \frac{\lambda}{18}}}$, and for $\lambda \ll g^2$, the critical temperature reduces to $T_c = 2\mu/g$. The effective potential has a non-zero minimum point below T_c as shown in Fig. 2, which changes continuously from zero to non-zero at T_c. Near the critical point, the effective potential has a discontinuous second derivative with respect to temperature,

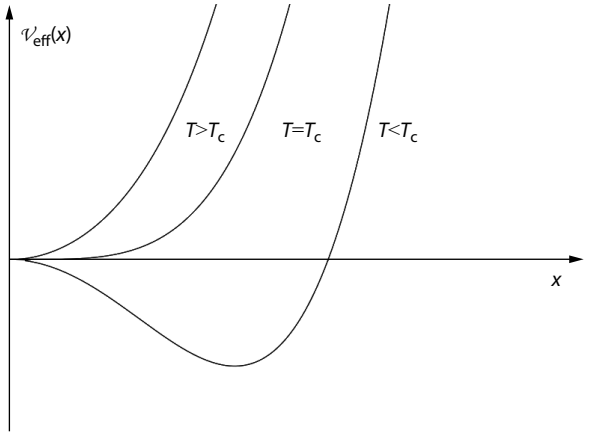

Fig. 2 The effective potential, divided by $\frac{3\mu^4}{2\lambda}$, at finite temperature including only thermal-mass corrections with $m_T^2/\mu^2 = 0.5, 1.0, 1.5$ and $\lambda < 3g^2 \ll 1$.

$$\lim_{T\to T_c}\mathcal{V}''_{\text{eff}}\left(T_c(1+t)\right) - \mathcal{V}''_{\text{eff}}\left(T_c(1-t)\right) = \lim_{T\to T_c}\frac{3g^2}{2\lambda}\left(\mu^2 - \frac{3}{4}g^2T^2\right) = \frac{3g^2\mu^2}{\lambda} \tag{39}$$

indicating the existence of a second-order phase transition. The related μ-T phase plane is divided into symmetrical phase and broken phases simply by T_c.

Considering the logarithmic term, the effective potential is given by

$$\mathcal{V}_{\text{eff}} = \left(\frac{1}{4}g^2T^2 - \mu^2\right)\varphi_{\text{cl}}^2 + \frac{\lambda}{6}\left[1 + \frac{9g^4}{8\pi^2\lambda}\left(\ln\frac{\lambda\varphi_{\text{cl}}^2}{3\mu^2} - \frac{1}{2}\right)\right]\varphi_{\text{cl}}^4 - \frac{\mu^2T^2}{6} \tag{40}$$

with

$$x = \frac{\lambda\varphi_{\text{cl}}^2}{3\mu^2}$$
$$a = 1 - \frac{9g^4}{16\lambda\pi^2} \tag{41}$$
$$b = 2 - \frac{g^2T^2}{2\mu^2} \in (-\infty, 2)$$

the effective potential is rewritten as a function of x,

$$\mathcal{V}_{\text{eff}} = \frac{3\mu^4}{2\lambda}x\left[(1-a)x + 2ax\ln x - b\right] \tag{42}$$

where T_c without the logarithmic term or $b_0 = 0$ is no longer the critical temperature, but the lower bound of the metastable region. The first and second derivatives of the effective potential with respect to φ_{cl} are

$$\frac{\partial\mathcal{V}_{\text{eff}}}{\partial\varphi_{\text{cl}}} = 2\mu^2\varphi_{\text{cl}}\left(x + 2ax\ln x - \frac{b}{2}\right) \tag{43}$$

$$\frac{\partial^2\mathcal{V}_{\text{eff}}}{\partial\varphi_{\text{cl}}^2} = \mu^2\left[(6+8a)x + 12ax\ln x - b\right] \tag{44}$$

The merging spinodal point is determined by simultaneously solving $V' = 0$ and $V'' = 0$, namely,

$$x + 2ax\ln x - \frac{b}{2} = 0 \tag{45}$$

$$(6+8a)x + 12ax\ln x - b = 0 \tag{46}$$

which gives the upper bound of the metastable region and the corresponding field value. After substituting $y = 1 + 2a\ln x$ into Eq. (45), using the Lambert W function ($z = W(z)e^{W(z)}$) yields $b_m = -x_m = -4a^{-(1+2a)/2a}$.

The critical point is reached when a local minimum of $\mathcal{V}_{\text{eff}}$ with $x \neq 0$ turns into a zero of the potential. This means that the following equation

$$(1-a)x + 2ax\ln x - b = 0 \tag{47}$$

which has only one solution at the minimum point. Solving Eq. (47) gives the critical point $b_c = f_{\min} = -2a\,e^{-(1+a)/2a}$ and the corresponding field value $x^\star = e^{-(1+a)/2a}$. V_{eff} versus $x^{1/2}$ at different temperatures are plotted in Fig. 3.

For $b > b_0$, $\mathcal{V}_{\text{eff}}$ shows a single minimum point $x = x^\star$ (Fig. 3a). At $b = b_0$, the maximum point $x = 0$ becomes unstable, and the system then goes into low-temperature metastable region (Fig. 3b). As shown by Fig. 3(d), the temperature range $b_m < b < b_c$ corresponds to the high-temperature metastable region, where the metastable phase is broken one $x = x^\star$.

https://doi.org/10.1007/s10118-026-3590-0

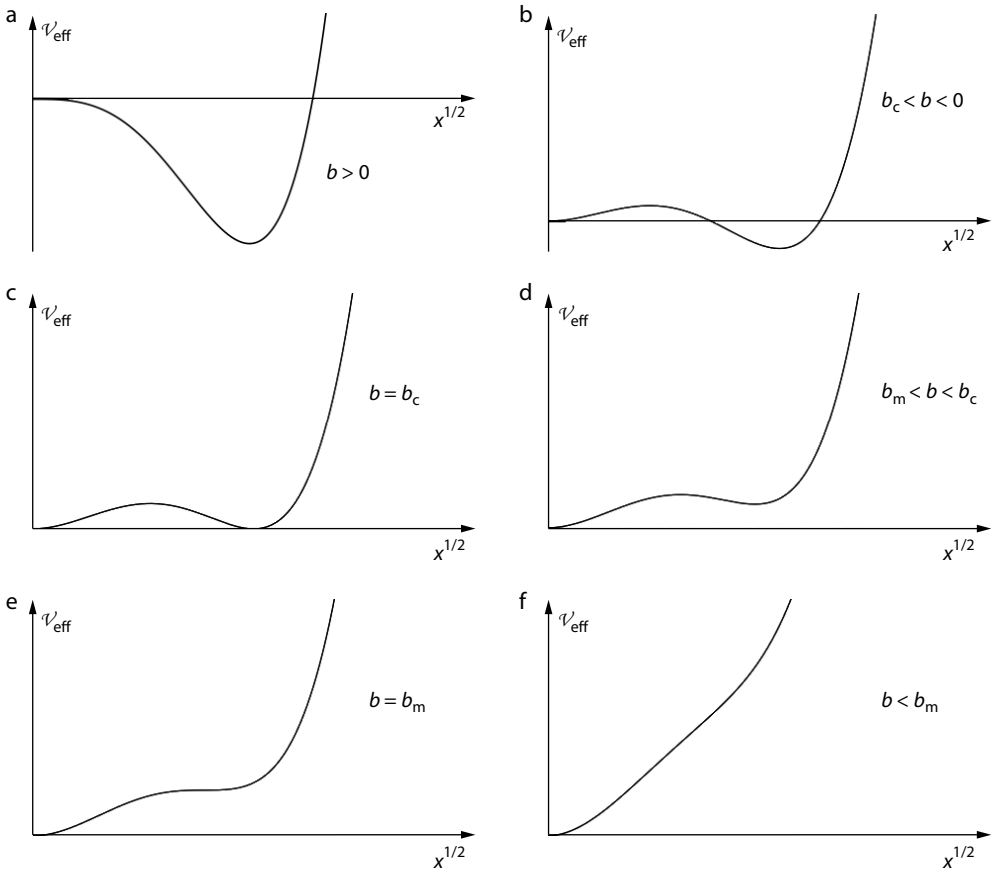

Fig. 3 The effective potential including the logarithmic term in the quartic coupling at different temperatures, with parameters $\mu = 1$, $a = 0.95$, and $\lambda = 1$. Panels correspond to: (a) $b > 0$, (b) $b_c < b < b_0$, (c) $b = b_c$, (d) $b_m < b < b_c$, (e) $b = b_m$, (f) $b < b_m$.

From Figs. 3(c) and 3(d) in the metastable region, the effective potential exhibits two minima and one maximum. The transition from the metastable to the stable state is governed by the potential barrier, characteristic of a nucleation mechanism driven by thermal fluctuations. b_c is the critical point where the minimal point shifts from $x = x^\star$ to $x = 0$ (Fig. 3c). It can be seen that around the critical point, the minimum of the order parameter discontinuous shifts from $x = x^\star$ to $x = 0$, indicating a first-order phase transition throughout the nucleation barrier. Similarly, the entropy change is

$$\Delta s = \mathcal{V}'_{\text{eff,min}}\left(b_c^-\right) - \partial\mathcal{V}_{\text{eff,min}}\left(b_c^+\right) = -\frac{3b\mu^4}{8a\lambda}\frac{\partial b}{\partial T} \tag{48}$$

Substituting $b_c = 2 - \dfrac{g^2T_c^2}{2\mu^2}$ and $b_c = 2ae^{-(1+a)/2a}$ yields

$$\Delta s = -\frac{3}{4}e^{-1/2a-1/2}\left(1 + ae^{-(1+a)/2a}\right)\frac{g^2}{\lambda}\frac{\mu^3}{g} \tag{49}$$

and the latent heat

$$\Delta h = T_c\,\Delta s = -\frac{\mu^4}{\lambda}\left[3e^{-(1+a)/2a}\left(1 + ae^{-(1+a)/2a}\right)\right] \tag{50}$$

It is evident that Δh is determined by λ, a and μ, but independent of b, which indicates the linear metastable boundary in the μ-T plane. For fixed arguments a, by decreasing g, the upper bound and critical lines shift down quickly because of $a \propto g^4$, while due to $T_0 \propto g^{-1}$, the the lower bound line does not rise up as rapidly as the upper bound line.

Considering ring resummation terms, the first order transition is also given. With $x^2 = \dfrac{\lambda\varphi_{\text{cl}}^2}{3\mu^2}$, the non-perturbative effective potential is expressed as below,

$$\begin{aligned}\mathcal{V}_{\text{eff}} = {} & \frac{3\mu^2}{\lambda}\left(\frac{g^2T^2}{4} - \mu^2\right)x^2 + \frac{3\mu^4}{2\lambda}x^4 \\ & + \frac{g^2\mu T^2}{32\pi}\left(3x^2 - 1\right)^{\frac{1}{2}} - \frac{T}{12\pi}\left[\mu^2\left(3x^2 - 1\right) + \frac{g^2T^2}{4}\right]^{\frac{3}{2}} \\ & + \frac{g^2\mu T^2}{32\pi}\left(x^2 - 1\right)^{\frac{1}{2}} - \frac{T}{12\pi}\left[\mu^2\left(x^2 - 1\right) + \frac{g^2T^2}{4}\right]^{\frac{3}{2}} \\ & + \frac{g^2\mu T^2}{16\pi}\left(\frac{6g^2x^2}{\lambda}\right)^{\frac{1}{2}} - \frac{T}{4\pi}\left[\frac{6g^2\mu^2x^2}{\lambda} + \frac{g^2T^2}{6}\right]^{\frac{3}{2}}\end{aligned} \tag{51}$$

For high temperature and long chain, and the order of coupling constants, only the last term of the gauge ring resummation is important. Thus, the effective potential can be further simplified to

$$\mathcal{V}_{\text{eff}} = \frac{3\mu^2}{\lambda}\left(\frac{g^2T^2}{4} - \mu^2\right)x^2 - \frac{T}{4\pi}\left(\frac{6g^2\mu^2x^2}{\lambda}\right)^{\frac{3}{2}} + \frac{3\mu^4}{2\lambda}x^4 \tag{52}$$

by $(1 + x)^{\frac{3}{2}} \sim 1 + \dfrac{3}{2}x$ for small x. The effective potential at different temperatures is plotted in Fig. 4(a). It can be observed that at $x = 0$, $\mathcal{V}_{\text{eff}}$ shifts from a maximum to a minimum, indicating a transition into the metastable region of the first-order transition. The phase diagram of the non-perturbative effective potential is shown in Fig. 4(b). The μ-T plane is divided into

https://doi.org/10.1007/s10118-026-3590-0

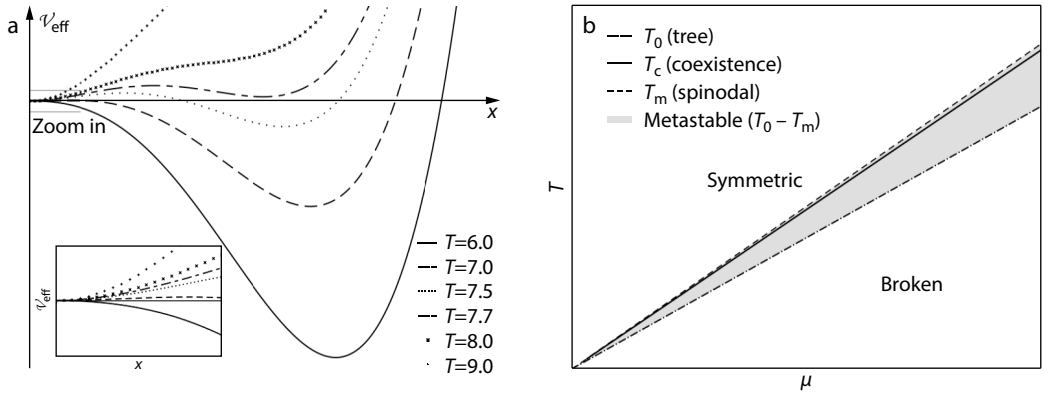

Fig. 4 (a) The non-perturbative effective potential at different temperatures and (b) the corresponding phase diagram with $\lambda = 0.01$, and $g^2 = 0.1$. Only the real part of the ring-resummation is retained, with $V_{\text{eff}}(x = 0)$ normalized to zero. The inset in (a) magnifies the region near $x = 0$. Setting $\mu = 1$ effectively rescales all parameters.

three regions, where the metastable region is marked with the shadowed area. It is unexpected to see that in this case, the critical lines are still linear and its dependence on g is similar with the logarithmic case.

The logarithmic and ring resummation terms cannot coexist. As the RG flow enters the regime $\lambda \ll g^2 < 1$ with non-negligible $\frac{g^4}{\lambda}$, the second-order transition changes into first-order one with metastable regions, which requires $g^2T^2 \sim \mu^2$ ($g \sim \beta\mu \ll 1$). However, under the constraint $\lambda \ll g^2$ within the high-temperature approximation, the coupling λ must be down to the order of 10^{-14} for $\beta g \sim 10^{-3}$. When the coupling $O(\lambda) \sim 10^{-14}$ is extremely weak, the mean-field value for logarithmic terms grows excessively, *i.e.*, $x \ll 1$, far beyond the classical scale, which is hard to exist as the aforementioned problem of parameter matching. Therefore, the phase transition induced by crystallization is supposed to be affected by the cubic term in the effective potential from non-perturbative thermal corrections, rather than the logarithmic vacuum energy modification.

In this way, the type of the phase transition is determined by g. Assuming that the coupling g can vary across orders of magnitude with relatively small λ, the variation of g can account for the emergence of long-range order in crystallization. g variation can explain the previously reported T^∞ in Gibbs-Thomson equation.[8,14] On the one hand, for large g, the ordering process is first-order, corresponding to the decrease of T^∞, and the corresponding heat is increased with increasing g. On the other hand, for the system going through crystallization with g decreasing significantly by α-relaxation, the ordering process is a second-order transition, and the corresponding heat is reduced at high enough temperatures which can not be measured.

The relaxation of the crystallized melt is also related to g variation in a similar way. Due to the g recovery before the disordering process, the later transition is first-order with large g. Thus a latent heat should be observed in the memory effect. The boundary temperature between domains I and IIa is related to the upper bound of metastable regions in this first-order transition. Increasing g can broaden domain IIa, which explains the entanglement dependence of boundary temperature between domains I and IIa.[27,30]

The implicit issue arises with the sequence of g variation in the above two phenomena. During crystallization, the coupling g either remains nearly unchanged or varies only slightly at first and then drops rapidly once symmetry breaking occurs. In the melting relaxation, g first grows large, with the broken symmetry restored only afterward, corresponding respectively to re-entanglement and the subsequent disordering process. Nevertheless, g undergoes a substantial change by α-relaxation, of which the microscopic motion pattern is exactly the soliton, related to the topological effect. This ordering is referred to the concept of topology protected by symmetry, namely, one vacuum state with a topological quantum number cannot be transformed into one unless the symmetry breaks.[62] However in this work, only the vibrations and the gauge couplings are included. The writhe and winding, and the translation of center of mass are not considered here, because the field model is an effective theory with Dirichlet boundary condition and random walk assumption, implying that a more complete theory related to more d.o.f. of the string should be considered.

Crystallization States Determined by Conservation Law

By crystallization, polymer changes from the amorphase state to the ordered crystal state, which allows a clear classification by the conservation of particles. The total particle number density n_0 is a conserved quantity given by Nother theorem, which includes both the μ-excited and background components, forming a particle reservoir and can be written as

$$n_0 = \lim_{V\to\infty} \frac{1}{V} \int \mathrm{d}^3x\, \mathcal{N}$$
$$\mathcal{N} = i\left(\varphi^\dagger \partial_0 \varphi - \partial_0 \varphi^\dagger \varphi\right) + 2A_0|\varphi|^2 \tag{53}$$

Applying the Matsubara frequency expansion $i\omega_k = 2\pi k/T$, $k \in \mathbb{Z}$ gives

$$\mathcal{N} = \sum\nolimits_k 2\omega_k|\varphi_k|^2 + 2A_0|\varphi|^2 \tag{54}$$

where the first term turns zero with the symmetry of summation over k. Assuming that A_0 is spatially uniform, the total number density is

$$n_0 = 2A_0 \lim_{V\to\infty} \int \frac{\mathrm{d}^3k}{(2\pi)^3} |\tilde{\varphi}(k)|^2 \tag{55}$$

This indicates that the temporal component of the gauge field acts as a chemical potential or background field.

The particles excited by μ corresponds to crystalline chains and thus is not conserved. The excited particle density can be derived from the derivative respect to μ of the effective potential $n = -\frac{\partial \mathcal{V}_{\text{eff}}}{\partial \mu}$. It can be further divided into condensed part or ordered part (n_c) related to the φ_{cl}-dependent terms in $\mathcal{V}_{\text{eff}}$ and thermally excited part or disordered part (n_{th}), as explained in the calculation of the effective potential.

Knowing n and n_0, the degrees of crystallinity and amorphous degree are defined as $X_c = \frac{n}{n_0}$, $X_a = 1 - X_c = 1 - \frac{n}{n_0}$. Hence, the detailed states include

- amorphase: $\mu = 0,\ n = 0$;
- supercooled amorphase: $\mu > 0,\ n = 0$;
- supercooled amorphase + disordered crystal: $n = n_{\text{th}} < n_0$;
- supercooled amorphase + disordered crystal + ordered crystal: $n = n_c + n_{\text{th}} < n_0$;
- supercooled amorphase + ordered crystal: $n = n_c < n_0$;
- pure disordered crystalline: $n = n_{\text{th}} = n_0$;
- ordered crystal + disordered crystal: $n = n_c + n_{\text{th}} = n_0$;
- ordered crystal: $n = n_c = n_0$.

As mentioned in Section **Renormalization Group**, O(2) symmetry is the most important feature of the random-walk string, where the folded-chain state is referred as the unbroken case. Thus, the ordered and disordered crystals correspond to the folded-chain and extended-chain crystals, respectively.

The observed persistence of supercooled amorphase indicates that there is the possible dynamic effect, which can be discussed cursorily with a phenomenological Gibbs free energy. The Gibbs free energy density of crystallized polymer is then generalized as $\mathcal{G} = \mu n + \mu_{\text{m}} n_0 + \mu_{\text{tp}}(n_0 - n)$. The first term represents the crystalline contribution, where μ can be chosen as Gibbs-Thomson type or double-potential well type for the crystalline-amorphase coexistence. The second term is the configurational entropy of crystalline-amorphase coexistence, where μ_{m} has a typical Flory-Huggins mixed free energy with the solution-solvent parameter set to zero. The third term corresponds to a possible topological contribution, assuming intuitively that only the amorphase carries nonzero topological charge $(n_0 - n)$. Since topological charge cannot arise from the instanton solution of the gauge field kinetic term in boundaryless Euclidean spacetime,[43,44,61] there might be an additional topological term in Lagrangian by dimensional reduction at finite temperature,[63] or other periodic boundary conditions.

CONCLUSIONS

In this work, polymer crystallizaiton is modeled considering the microscopic dynamics symmetry, which is described by self-avoiding random string field theory with gauged O(N) symmetry in dimension $d = 3 + 1$ with $N = 2$. Within this model, the SO(N) gauge field accounts for the entanglement in the bulk. The number of replica components N is fixed at 2 by the requirement of infrared stability and unconfined charge, thus this scalar-gauge theory is simplified to Coleman-Weinberg model. By invoking SSB induced by crystallizaiton, this model is extended to the grand canonical ensemble at finite temperature, with the chemical potential representing crytals. With the modification of ring resummation and large gauge coupling constants g, the formation mechanism of the long-range order changes from the second-order phase transition at zero temperature into a weak first-order transition with metastable region. This g dependence of the long-range order improves the unstanding on the variation of extrapolated temperatures in Gibbs-Thomson equation and, the reentanglement and disorientation in melt relaxation. Morevoer, a clear definition of crystallinity is derived from the developed scalar conservation, which is controlded by the chemical potential μ in the grand canonical ensemble. This effective U(1) scalar-gauge theory also provides the available model for more degrees of freedom that is referred to the chain's writhe, winding and the whole chain's translation.

Conflict of Interests

The authors declare no interest conflict.

REFERENCES

1 Peskin, M. E. in *An introduction to quantum field theory*, Westview Press, Boulder, CO, **2018**, pp. 323–330, 352–383, 406–431, 469–544.
2 Landau, L. D.; Lifshitz, E. M. in *Statistical physics. I* (in Chinese), Higher Education Press, Beijing, **2011**, pp. 347–350, 386–427.
3 Strobl, G. Colloquium: laws controlling crystallization and melting in bulk polymers. *Rev. Mod. Phys.* **2009**, 81, 1287–1300.
4 Sadler, D. M.; Gilmer, G. H. Rate-theory model of polymer crystallization. *Phys. Rev. Lett.* **2009**, 56, 2708.
5 Sadler, D. M. New explanation for chain folding in polymers. *Nature* **1987**, 326, 174–177.
6 DiMarzio, E. A.; Guttman, C. M. Polymer crystallization: proper accounting of a wider class of paths to crystallization—variations on a theme of point. *J. Appl. Phys.* **1982**, 53, 6581–6590.
7 Mandelkern, L. in *Crystallization of polymers: volume 2, kinetics and mechanisms*, Cambridge University Press, New York, NY, **2004**, pp. 1–154.
8 Schulz, M.; Seidlitz, A.; Kurz, R.; Bärenwald, R.; Petzold, A.; Saalwächter, K.; Thurn-Albrecht, T. The underestimated effect of intracrystalline chain dynamics on the morphology and stability of semicrystalline polymers. *Macromolecules* **2018**, 51, 8377–8385.
9 Hu, W. G.; Schmidt-Rohr, K. Polymer ultradrawability: the crucial role of α-relaxation chain mobility in the crystallites. *Acta Polym.* **1999**, 50, 271–285.
10 Qiu, X.; Hu, C. L.; Li, J. Q.; Huang, D. H.; Jiang, S. C. Role of conformation in crystal formation and transition of polybutene-1. *CrystEngComm* **2019**, 21, 4243–4249.
11 Dong, B. B.; Yang, X. K.; Ji, Y. X.; Su, F. M.; Shao, C. G.; Liu, C. T. Polymorph selection during melt crystallization of the isotactic polybutene-1 homopolymer depending on the melt state and crystallization pressure. *Soft Matter* **2020**, 16, 9074–9082.
12 Qin, Y. N.; Song, W. B.; Chen, M.; Litvinov, V.; Men, Y. F. Chain entanglements and interlamellar links in isotactic polybutene-1: The effect of condis crystals and crystallization temperature. *Macromolecules* **2022**, 55, 5636–5644.
13 Ni, L. L.; Sun, C. X.; Xu, S. S.; Xiang, W. K.; Pan, Y. W.; Wang, B.; Zheng, Y.; Yu, C. T.; Pan, P. J. Thermally induced phase transition

Graphical Abstract

Spontaneous Gauged O(*N*) Symmetry Breaking in Polymer Crystallization

Mai Zhou, Gui-Qiu Ma, and Zhe Ma

Tianjin University

The Self-Avoiding String in polymer melts corresponds to O(*N*) × U(1) symmetry. Crystallization (chemical potential) induces its breaking into Z_2, while entanglements act as gauge fields, shifting the ordering process from a second-order to a first-order phase transition.

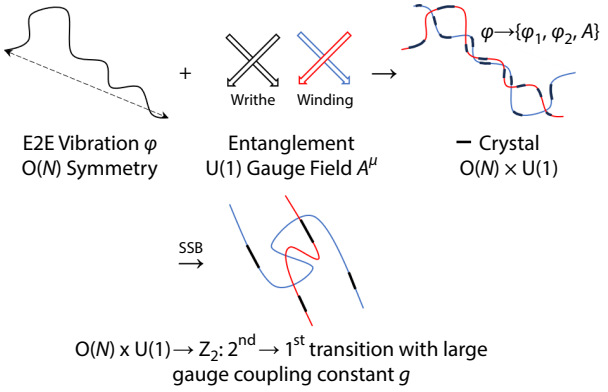

Chinese J. Polym. Sci., 2026 *https://doi.org/10.1007/s10118-026-3590-0*

of polybutene-1 from form I' to form II through melt recrystallization: crucial role of chain entanglement. *Macromolecules* **2023**, 56, 1973–1982.

14 Hauser, G.; Schmidtke, J.; Strobl, G. The role of co-units in polymer crystallization and melting: new insights from studies on syndiotactic poly (propene-*co*-octene). *Macromolecules* **1998**, 31, 6250–6258.

15 Hikosaka, M.; Watanabe, K.; Okada, K.; Yamazaki, S. in *Interphases and mesophases in polymer crystallization III*, Springer, Berlin, Heidelberg, **2005**, pp. 137–186.

16 Schulz, M.; Seidlitz, A.; Petzold, A.; Thurn-Albrecht, T. The effect of intracrystalline chain dynamics on melting and reorganization during heating in semicrystalline polymers. *Polymer* **2020**, 196, 122441.

17 Luo, C. F.; Sommer, J. U. Growth pathway and precursor states in single lamellar crystallization: MD simulations. *Macromolecules* **2011**, 44, 1523–1529.

18 Ewen, B.; Richter, D. Neutron spin echo investigations on the segmental dynamics of polymers in melts, networks and solutions. *Neutron Spin Echo Spectroscopy* **1999**, 134, 1–129.

19 Rybnikar, F.; Carter, J. D.; Geil, P. H. Folded chain lamellar crystal self-decoration of extended chain crystals of a random terpolymer main chain liquid crystal polymer. *J. Macromol. Sci., Part A* **1995**, 32, 1133–1138.

20 Miyoshi, T.; Mamun, A.; Reichert, D. Fast dynamics and conformations of polymer in a conformational disordered crystal characterized by ^{1}H-^{13}C wise NMR. *Macromolecules* **2010**, 43, 3986–3989.

21 Qin, Y. N.; Qiao, Y. N.; Chassé, W.; Litvinov, V.; Men, Y. F. Crystallinity of polyolefins with large side groups by low-field ^{1}H NMR T_2 relaxometry: isotactic polybutene-1 with form II and I crystals. *Solid State Nucl. Magn. Reson.* **2020**, 105, 101637.

22 Jin, F.; Yuan, S. C.; Wang, S. J.; Zhang, Y.; Zheng, Y.; Hong, Y. L.; Miyoshi, T. Polymer chains fold prior to crystallization. *ACS Macro Lett.* **2022**, 11, 284–288.

23 Miura, T.; Kishi, R.; Mikami, M. Simulation study of the order formation dynamics in the melt crystallization of flexible chain molecules induced by rigid molecular nuclei. *J. Chem. Phys.* **2003**, 119, 6354–6360.

24 Guttman, C. M.; DiMarzio, E. A.; Hoffman, J. D. Modelling the amorphous phase and the fold surface of a semicrystalline polymer—the gambler's ruin method. *Polymer* **1981**, 22, 1466–1479.

25 Mansfield, M. L. A continuum gambler's ruin model. *Macromolecules* **1988**, 21, 126–130.

26 Adhikari, S.; Muthukumar, M. Theory of statistics of ties, loops, and tails in semicrystalline polymers. *J. Chem. Phys.* **2019**, 151, 114905.

27 Yamazaki, S.; Gu, F. M.; Watanabe, K.; Okada, K.; Toda, A.; Hikosaka, M. Two-step formation of entanglement from disentangled polymer melt detected by using nucleation rate. *Polymer* **2006**, 47, 6422–6428.

28 Chen, R.; Jiang, S. M.; Luo, C. F. Reconstruction of the entanglement network and its effect on the crystallization and mechanical strength of sintered polymers. *Macromolecules* **2023**, 56, 5237–5247.

29 Sangroniz, L.; Cavallo, D.; Müller, A. J. Self-nucleation effects on polymer crystallization. *Macromolecules* **2020**, 53, 4581–4604.

30 Liu, X.; Yu, W. Role of chain dynamics in the melt memory effect of crystallization. *Macromolecules* **2020**, 53, 7887–7898.

31 Doi, M.; Edwards, S. F. Dynamics of concentrated polymer systems. Part 1.—Brownian motion in the equilibrium state. *J. Chem. Soc., Faraday Trans. 2* **1978a**, 74, 1789–1801.

32 Doi, M.; Edwards, S. F. Dynamics of concentrated polymer systems. part 2.—molecular motion under flow. *J. Chem. Soc., Faraday Trans. 2* **1978b**, 74, 1802–1817.

33 Flory, P. J. Thermodynamics of crystallization in high polymers. iv. a theory of crystalline states and fusion in polymers, copolymers, and their mixtures with diluents. *J. Chem. Phys.* **1949**, 17, 223–240.

34 Mansfield, M. L. Change in radius of gyration of semicrystalline polymers upon crystallization. *Macromolecules* **1986**, 19, 851–854.

35 Mansfield, M. L. Temperature-dependent changes in the structure of the amorphous domains of semicrystalline polymers. *Macromolecules* **1987**, 20, 1384–1393.

36 Rieger, J.; Mansfield, M. L. Comments on "Temperature-dependent changes in the structure of the amorphous domains

of semicrystalline polymers". *Macromolecules* **1989**, 22, 3810−3812.
37 Iwata, K. Local knot model of entangled polymer chains. 2. theory of probe fluctuation and diffusion coefficient of a single local knot. *J. Phys. Chem.* **1992**, 96, 4111−4118.
38 Iwata, K. Role of entanglement in crystalline polymers 1. Basic theory. *Polymer* **2002**, 43, 6609−6626.
39 Olmsted, P. D.; Poon, W. C. K.; McLeish, T. C. B.; Terrill, N. J.; Ryan, A. J. Spinodal-assisted crystallization in polymer melts. *Phys. Rev. Lett.* **1998**, 81, 373.
40 Yakunin, A. N. A study of critical phenomena and dissipative nanostructures in self-organizing polymer systems. *Polym. Sci. Ser. A* **2012**, 54, 155−164.
41 des Cloizeaux, J. The lagrangian theory of polymer solutions at intermediate concentrations. *J. Phys.* **1975**, 36, 281−291.
42 des Cloizeaux, J.; Jannink, G. in *Polymers in solution: their modelling and structure*, Oxford University Press, New York, NY, **1991**, pp. 431–448.
43 Polyakov, A. M. in *Gauge fields and strings*, Taylor & Francis, New York, NY, **2018**, pp. 15–17, 49–71, 85–100.
44 Schwarz, A. S. in *Quantum field theory and topology*, Springer, New York, NY, **2013**, pp. 80–194.
45 Baez, J. C.; Muniain, J. P. in *Gauge fields, knots and gravity*, World Scientific, Singapore, **1994**, pp. 159–353.
46 Vilgis, T. A. Polymer theory: path integrals and scaling. *Phys. Rep.* **2000**, 336, 167−254.
47 Kim, K.-S.; Dutta, S.; Jho, Y. Entangled polymer complexes as higgs phenomena. *Soft Matter* **2015**, *11*, 7932−7941.
48 Ferrari, F.; Lazzizzera, I. Polymer topology and Chern-Simons field theory. *Nucl. Phys. B* **1999**, 559, 673−688.
49 Ferrari, F. A new strategy to microscopic modeling of topological entanglement in polymers based on field theory. *Nucl. Phys. B* **2019**, 948, 114778.
50 Luo, C. F.; Sommer, J. U. Frozen topology: Entanglements control nucleation and crystallization in polymers. *Phys. Rev. Lett.* **2014**, 112, 195702.
51 Lu, H. F.; Zhou, Z. P.; Hao, T. F.; Ye, X. B.; Ne, Y. J. Temperature dependence of structural properties and chain configurational study: a molecular dynamics simulation of polyethylene chains. *Macromol. Theory Simul.* **2015**, 24, 335−343.
52 Le Bellac, M. in *Thermal field theory*, Cambridge University Press, Cambridge, **2000**, pp. 44–46, 62–77, 118–123.
53 Shaw, M. T.; MacKnight, W. J. in *Introduction to polymer viscoelasticity*, Wiley, New Jersey, NJ, **2018**, pp. 51–97.
54 Fu, Q.; Heck, B.; Strobl, G.; Thomann, Y. A temperature-and molar mass-dependent change in the crystallization mechanism of poly (1-butene): transition from chain-folded to chain-extended crystallization? *Macromolecules*, **2001**, *34*, 2502−2511.
55 Su, F. M.; Li, X. Y.; Zhou, W. M.; Chen, W.; Li, H. L.; Cong, Y. H.; Hong, Z. H.; Qi, Z. M.; Li, L. B. Accelerating crystal-crystal transition in poly (1-butene) with two-step crystallization: an *in-situ* microscopic infrared imaging and microbeam x-ray diffraction study. *Polymer* **2013**, 54, 3408−3416.
56 Su, F. M.; Li, X. Y.; Zhou, W. M.; Zhu, S. S.; Ji, Y. X.; Wang, Z.; Qi, Z. M.; Li, L. B. Direct formation of isotactic poly (1-butene) form I crystal from memorized ordered melt. *Macromolecules* **2013**, 46, 7399−7405.
57 Chen, J. L.; Wang, B. H.; Sun, T. C.; Xu, J. W.; Chen, J. B.; Zhang, B. Transformation from form II to form I accelerated by oriented lamellae in polybutene-1. *Polymer* **2019**, 185, 121966.
58 Kurihara, H.; Kitade, S.; Ichino, K.; Akiba, I.; Sakurai, K. Elongation induced β- to α-crystalline transformation and microvoid formation in isotactic polypropylene as revealed by time-resolved WAXS/SAXS. *Polym. J.* **2019**, 51, 199−209.
59 Zhang, J. Q.; Liu, C.; Zhao, X. T.; Zhang, Z. J.; Chen, Q. Formation of fibrillar crystals strongly accelerates the form II to I transformation of polybutene-1. *Soft Matter* **2020**, 16, 4955−4960.
60 Lu, Y. G.; Wang, B. H.; Jia, N.; Chen, J. B.; Shen, C. Y.; Zhang, B. Crystallization studies on heterogeneous melts of polybutene-1. *Polymer* **2022**, 261, 125408.
61 Weinberg, S. in *The quantum theory of fields, volume II*, Cambridge University Press, Cambridge, **1995**, pp. 332–352, 450–455.
62 Syi, J.; Mansfield, M. L. Soliton model of the crystalline α-relaxation. *Polymer* **1988**, 29, 987−997.
63 Chen, X.; Liu, Z. X.; Wen, X. G. Two-dimensional symmetry-protected topological orders and their protected gapless edge excitations. *Phys. Rev. B* **2011**, 84, 235141.
64 Fosco, C. D.; Schaposnik, F. A. Induced Chern-Simons term by dimensional reduction. *Phys. Rev. D* **2022**, 105, 105023.

https://doi.org/10.1007/s10118-026-3590-0